Consequences of the constitutive NOX2 activity in living cells: Cytosol acidification, apoptosis, and localized lipid peroxidation

Hana Valenta, Sophie Dupre-Crochet, Mouna Abdesselem, Tania Bizouarn, Laura Baciou, Oliver Nüsse, Ariane Deniset-Besseau, Marie Erard

To cite this version:

Hana Valenta, Sophie Dupre-Crochet, Mouna Abdesselem, Tania Bizouarn, Laura Baciou, et al.. Consequences of the constitutive NOX2 activity in living cells: Cytosol acidification, apoptosis, and localized lipid peroxidation. Biochimica et Biophysica Acta - Molecular Cell Research, 2022, 1869 (9), pp.119276. 10.1016/j.bbamcr.2022.119276 . hal-03858717

HAL Id: hal-03858717
https://hal.science/hal-03858717v1

Submitted on 22 Jul 2024

Version of Record: https://www.sciencedirect.com/science/article/pii/S0167488922000672
Manuscript_e6001d5805b02777da4e17b349087952

Consequences of the constitutive NOX2 activity in living cells: cytosol acidification, apoptosis, and localized lipid peroxidation

Hana Valenta[a], Sophie Dupré[a], Mouna Abdesselem[a], Tania Bizouarn[a], Laura Baciou[a], Oliver Nüsse[a], Ariane Deniset-Besseau[a], Marie Erard[a]*

[a] *Institut de Chimie Physique, UMR8000, Université Paris-Saclay, CNRS, 91405 Orsay, France*

Corresponding author: marie.erard@universite-paris-saclay.fr

Highlights:

- Trimera is a tool to trigger a continuous ROS production in living cells
- Continuous NOX2 activity causes cytosol acidification and apoptosis
- ROS overproduction leads to localized oxidation of the membrane lipids
- Trimera tends to clusterize in the plasma membrane of COSNOX and COS-7 cells

Abstract:

The phagocyte NADPH oxidase (NOX2) is a key enzyme of the innate immune system generating superoxide anions ($O_2^{\bullet-}$), precursors of reactive oxygen species. The NOX2 protein complex is composed of six subunits: two membrane proteins (gp91^{phox} and p22^{phox}) forming the catalytic core, three cytosolic proteins (p67^{phox}, p47^{phox} and p40^{phox}) and a small GTPase Rac. The sophisticated activation mechanism of the NADPH oxidase relies on the assembly of cytosolic subunits with the membrane-bound components. A chimeric protein, called 'Trimera', composed of the essential domains of the cytosolic proteins p47^{phox} (aa 1-286), p67^{phox} (aa 1-212) and full-length Rac1Q61L, enables a constitutive and robust NOX2 activity in cells without the need of any stimulus. We employed Trimera as a single activating protein of the phagocyte NADPH oxidase in living cells and examined the consequences on the cell physiology of this continuous and long-term NOX activity. We showed that the sustained high level of NOX activity causes acidification of the intracellular pH, triggers apoptosis and leads to local peroxidation of lipids in the membrane. These local damages to the membrane correlate with the strong tendency of the Trimera to clusterize in the plasma membrane observed by FRET-FLIM microscopy.

Keywords: NADPH oxidase, ROS, oxidative stress, intracellular pH, lipid peroxidation, FRET-FLIM

Abbreviations: aa, amino acid; AFM, Atomic Force Microscopy; DPI, Diphenylene Iodonium; FRET, Förster Resonance Energy Transfer; FLIM, Fluorescence-Lifetime Imaging Microscopy; FP, Fluorescent Protein; HRP, Horseradish Peroxidase; IR, Infra-Red; NADPH, Nicotinamide Adenine Dinucleotide Phosphate reduced form; NMDG, N-Methyl-D-glucamine; PMA, Phorbol 12-Myristate 13-Acetate; ROI, Region of Interest; ROS, Reactive Oxygen Species

Acknowledgments:

COS^{p22} and COS$^{gp91\text{-}p22}$ cells also called COSNOX cells were a kind gift from Mary C. Dinauer (Washington University School of Medicine, USA). The plasmid of the Trimera was a generous gift from E. Pick (Tel Aviv University, Israel). H.V. was supported by a PhD fellowship form MESRI. This work has benefited from the SpICy microscopy facility of ICP for TSCPC-FLIM measurements and flow cytometry and the Light Microcopy Facility Imagerie-Gif for confocal microscopy.

1. INTRODUCTION

The NOX family of NADPH oxidases generates superoxide anion ($O_2^{\bullet -}$) that is the precursor of other reactive oxygen species (ROS) [1]. Among them, the phagocyte NADPH oxidase (NOX2), is the best known and a prototype for other family members. It is a key player of the most effective mechanisms for the destruction of pathogenic microorganisms by the ROS production. This NADPH oxidase is a protein complex composed of six subunits; two membrane proteins ($gp91^{phox}$ and $p22^{phox}$) forming the catalytic core, three regulatory proteins ($p67^{phox}$, $p47^{phox}$ and $p40^{phox}$) forming a ternary complex and a small GTPase Rac [1]. Lack of the NOX2 activity leads to chronic granulomatous disease (CGD) characterized by severe and recurrent infections. On the other hand, ROS overproduction contributes to cardiovascular and neurodegenerative diseases. Thus, the NOX2 activity needs to be finely regulated in order to produce the ROS where and when they are needed and in an appropriate concentration; either as antimicrobial effectors or as signaling molecule [2],[3]. The activity of the NADPH oxidase is controlled by the spatial separation of its membrane components from the cytosolic subunits. Upon activation either by phagocytosis or by a soluble stimulus such as phorbol ester (PMA) or arachidonic acid, the cell signaling cascade triggers phosphorylations of the ternary complex of cytosolic subunits. Those phosphorylations change dramatically its conformation into an active state able to interact with the membrane. Then the ternary complex migrates to the membrane independently of Rac. When it reaches the membrane, it associates with $gp91^{phox}$, $p22^{phox}$ and Rac-GTP forming the active complex able to produce superoxide anions. The formation of the active complex involves the reorganization of the intramolecular interactions within the cytosolic complex and formation of new interactions with the membrane subunits as well as with membrane lipids [4].

Berdichevsky *et al.* designed fusion proteins of selected regions of cytosolic proteins $p67^{phox}$ and $p47^{phox}$ with Rac [5]. The chimeric protein called Trimera is composed of the PX domain and the two SH3 domains of $p47^{phox}$ (aa 1-286), the TPR domains and the activation domain of $p67^{phox}$ (aa 1-212) and the full-length Rac1 containing the Q61L mutation assuring that Rac1 is in the active GTP-bound form (Figure 1) [5]. We recently observed that such a chimeric protein composed of the domains of cytosolic subunits, which are essential for the NADPH oxidase activity, turns the NADPH oxidase into a constitutively active enzyme in live cells [6]. The Trimera offers the opportunity to investigate the NADPH oxidase activity independently from any stimulation of the cellular signaling cascades. It is thus possible to focus on the active state of the NADPH oxidase and the consequences of long-term ROS production at the molecular level. In this article, we describe the localization and distribution of the Trimera at the subcellular level in the cell membrane using fluorescent protein labeled Trimera. We likewise evaluated the consequences of the continuous and long-term NADPH oxidase activity on cell physiology in terms of cell viability, intracellular pH and lipid peroxidation.

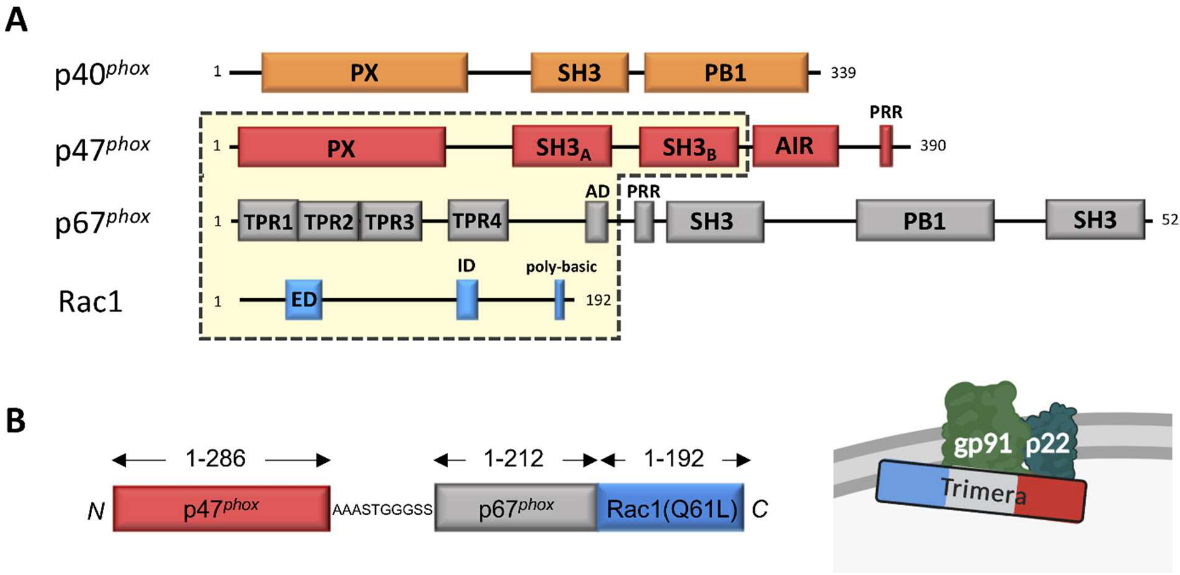

__Figure 1. A: Modular structure of the cytosolic subunits and Rac1.__ The modules (domains) are represented by boxes whose size is proportional to the number of involved amino acid residues. AD is the activation domain, PRR is the prolin rich region, ED is the effector domain, ID is the insert domain. Domains in the yellow rectangle are conserved in the Trimera. __B: Chimeric protein "Trimera".__ Left: Trimera is a fusion protein created from the functionally important domains of $p47^{phox}$, $p67^{phox}$ *and Rac1 (showed in A). Rac1 contains the point mutation Q61L, which keeps it in a GTP-bound form. AAASTGGGSS is a 10-amino acid linker between the* $p47^{phox}$ *and* $p67^{phox}$ *segments. There is no linker between* $p67^{phox}$ *and Rac1. Right: Trimera can create the active NOX complex with* $gp91^{phox}$ *and* $p22^{phox}$*. Trimera is a single activating protein that can replace separated cytosolic proteins in the NOX activation process.*

2. MATERIALS AND METHODS

2.1. Materials

Horseradish peroxidase (HRP), phorbol 12-myristate 13-acetate (PMA), N-Methyl-D-glucamine (NMDG), nigericin and methyl-beta-cyclodextrin were purchased from Sigma-Aldrich (St Quentin, France). Dulbecco's PBS (DPBS) and all cell culture media were purchased from Gibco (France). Annexin V APC and propidium iodide (PI) were purchased from Invitrogen (France). Primary antibody anti-4-HNE was purchased from Abcam (mouse, ab48506). Secondary antibody conjugated to Alexa Fluor 647 was purchased from Thermo Fisher Scientific.

2.2. Plasmid library

The plasmid coding for the Citrine-Trimera fusion protein was prepared in our laboratory as described previously [6]. The orginal GFP fused Trimera plasmid was a kind gift of E. Pick [7]. This plasmid was then used for creating mTurquoise-Trimera by exchanging the fluorescent protein tag. Citrine-Trimera and plasmid of mTurquoise (vector, originally pECitrineC1) were digested with *Hind*III and *Kpn*I and ligated using standard protocols. The sequence of the resulting plasmid was verified by sequencing (Genewiz, Germany). Endotoxin free plasmid, which is more convenient for cell transfection, was prepared using the EndoFree Plasmid Maxi Kit (Qiagen, France). For FRET-FLIM experiments, a plasmid of mCitrine-Trimera with monomeric Citrine (A206K mutation) was prepared. Using QuikChange Lightning Multi Site-Directed Mutagenesis Kit (Agilent) and following primers: forward 5'-cctgagctaccagtccaagctgagcaaagaccccc-3' and reverse 5'-ggggtctttgctcagcttggactggtagctcagg-3', A206K mutation was introduced in the DNA sequence of Citrine. We ordered the single point mutations from Eurofins (Germany) to obtain two mutated versions of Rac1Q61L (dominant positive) originally present in the plasmid coding for mTurquoise-Trimera: the wild type version of Rac1 (Rac1 61Q) and the dominant negative version of Rac1, Rac1 T17N [8].

2.3. Cell culture and transfection

COS^{p22} [8] and COS$^{gp91\text{-}p22}$ [9] cells were a gift from Mary Dinauer. COS$^{gp91\text{-}p22}$ cells are called COSNOX. Stock cultures of cells (COS-7 (African Green monkey kidney), COS^{p22} and COSNOX) were maintained at 37°C in DMEM supplemented with 10% fetal bovine serum (FBS) in a humidified atmosphere containing 5% CO_2. The culture medium of COS^{p22} and COS$^{gp91\text{-}p22}$ cells was supplemented with the selecting antibiotics Geneticin (1.8 mg/mL, Thermo Fisher Scientific) and Puromycin (1 µg/mL, Sigma Aldrich) to maintain the expression of p22^{phox} and gp91^{phox} respectively. The day before transfection, cells were seeded in selected plates (Greiner Bio-one) and transfected at 80–90% of confluency using X-tremeGENE™ HP DNA Transfection Reagent (Roche) following strictly the manufacturer protocol.

2.4. *In-cell* NADPH oxidase activity assay

The NADPH oxidase activity was measured by luminescence assay. The COSNOX cells were plated in 24-well plates and transfected 24 h before experiment. Transfection efficiency was verified first by wide-field microscopy and then by flow cytometry (Figure S1). Only cells with the same level of transfection were used for the luminescence assay in order to directly compare the ROS production. The assay was performed in PSBG buffer (PBS supplemented with 0.5 mM $MgCl_2$, 0.9 mM $CaCl_2$, and 7.5 mM glucose) at 35°C using SynergyH1 plate reader (Biotek, USA). L-012 (100 µM, Wako Chemicals) and HRP (20 U/ml) were mixed and added to the wells containing transfected COSNOX cells. If needed, PMA (1 µM) was added to induces the NADPH oxidase activation process 2 min after addition of L-012 and HRP. 25 µM of DPI was added to stop the $O_2^{\bullet-}$ production. The ROS production was quantified as integrated luminescence over time. The latter one is normalized by the percentage of transfected cells in the sample evaluated by flow cytometry. For Figure 2E, the integrated luminescence was also normalized by the expression level estimated by flow cytometry (average fluorescence intensity of fluorescent cells).

2.5. pH measurements

A stock solution of SNARF-1 was prepared in DMSO at a concentration of 5 mM and kept at -20 °C.

Cells were seeded in 12-well plates and prior to loading with SNARF-1, the supplemented DMEM was removed and cells were washed with PBS. To load SNARF-1, cells were incubated with 5 µM SNARF-1 for 30 min in PBS at 37°C, 5% CO_2. Loading was done in PBS buffer to avoid unwanted hydrolysis by esterase present in serum. After incubation, cells were centrifuged (5 min, 1200 rpm), resuspended in PBS and analyzed by flow cytometry. SNARF-1 calibration was performed *in-cell* according to the following method. After incubation with the fluorescent probe, cells were resuspended in buffers containing 15 mM MES, 15 mM HEPES and 140 mM KCl at various pH values (6.0-8.0). The addition of 15 µM nigericin (10 min, RT) allowed an exchange of K^+ for H^+ resulting in a rapid equilibration of external and internal pH. The calibration curve varied slightly for each experiment and thus was repeated for each experiment. A typical example is shown in Figure S2.

To exclude any contribution of the Na^+/H^+ exchanger, some of the experiments were performed in Na^+-free medium containing: 140 mM NMDG-Cl, 5 mM KCl, 1 mM $MgCl_2$, 1.8 mM $CaCl_2$, 10 mM HEPES and 10 mM glucose at pH 7.4 [10]. In this case, cells were first incubated in NMDG buffer for 30 min (37°C, 5% CO2) and then they were loaded by SNARF-1 diluted in the NMDG buffer (30 min, 37°C, 5% CO2). After that, the cells were detached, centrifuged (5 min, 1200 rpm), resuspended in DPBS and analyzed by flow cytometry.

2.6. Apoptosis tests

The cells were seeded in 12-well plates and analyzed 24 h after transfection. Prior to analysis, they were washed with PBS and detached with trypsin (Gibco). For apoptosis tests, cells were resuspended in annexin binding buffer (Invitrogen) containing Ca^{2+} due to the calcium dependence of the Annexin V:PS interaction. Cells were incubated with Annexin V APC for 10 min at RT and analyzed by flow cytometry.

2.7. Lipid peroxidation investigated by InfraRed (IR) spectro-microscopy

COSNOX and COS-7 cells for IR analysis were grown on the CaF_2 cover slips in 24-well plates. 24 h hours after transfection (DNA amount: Citrine-Trimera 0,5 µg/well, Citrine-Trimera++ 1,5 µg/well), they were fixed by 4% paraformaldehyde, washed using PBS/water baths to successively decrease the amount of PBS (going from 100% PBS to 100% water) and stored at 4°C before analysis.

2.7.1 Global analysis by IR microspectroscopy

At least 20 cells per condition were examined by IR microspectroscopy (µFTIR). During IR imaging, transmission type spectra were recorded by a LUMOS microspectrophotometer (8x / 0,6 NA Cassegrain objective), Bruker Optik, GmbH system coupled to a liquid nitrogen cooled MCT detector. A square aperture of 20 µm side length restricted the sample area illuminated by the IR radiation. Transmission type IR spectra were acquired from 4000 to 800 cm^{-1} at a spectral resolution of 4 cm^{-1}.

2.7.2 Subcellular analysis by IR nanospectroscopy, AFM-IR

At least 7 fixed cells per condition from 2 independent experiment were examined using IR nanospectroscopy, AFM-IR system. In this technique, the AFM tip is in contact with the sample and detects its thermal expansion induced by the absorption of the IR source. The instrument used in this study is a NanoIR2 (Anasys Instrument, Bruker nano Surfaces, California, USA) combining an AFM set-up in contact mode with an IR pulsed tunable laser covering the mid-IR region from 1945-890 cm^{-1} (QLC beam, MIRcat-QT, DAYLIGHT solutions; peak powers up to 1 W; average power up to 0.5 W, wavelength repeatability < 0.1 cm^{-1} and a tunable repetition rate of 1-2000 kHz). We used a scan rate of 0.5 Hz per line in the contact mode. An Au-coated silicon cantilever (Mikromasch) with a nominal tip radius < 15 nm and a spring constant between 0.03 and 0.2 N/m was used for all measurements (scan rate between 0.1 and 0.3 Hz per line, laser power 9.79 %, pulse width 160 to 200 ns, pulse rate of the 4th mode around 700 kHz, PLL (phase locked-loop)). The AFM-IR spectra were collected with a data point spacing of 1 cm^{-1}, sweep rate 200 cm^{-1}/s, average on 4 spectra at each position over the spectral range 900–1900 cm^{-1}.

All experiments were performed at room temperature in purged air. The data were analyzed in Orange software for baseline correction (linear), gaussian smoothing (SD 5), area normalization (full range) and in MountainMaps software 9.0 for profilometry analysis, topography and IR-map analysis. Orange is a comprehensive, component-based software suite for machine learning and data mining, developed at Bioinformatics Laboratory, Faculty of Computer and Information Science, University of Ljubljana, Slovenia [11]. MountainMaps 9.0 was developed by Digital Surf, Besançon, France.

2.8. Immunostaining assay

COSNOX cells were seeded on glass cover slips in a 12-well plate in complete DMEM medium and transfected according to the manufacturer's protocol. 24 h after transfection, the cells were fixed with 4% paraformaldehyde (Electron Microscopy Sciences) and kept 45 min at 13°C. After washing with PBS buffer, cells were incubated 10 min at RT with 1% glycine (Sigma). Cells were permeabilized by 0.1% saponin (Rectapur Prolabo) diluted in DPBS, 3x 5 min at RT. Afterwards, cells were incubated with DPBS containing 10% FBS and 0.1% saponin for 30 min at RT. The permeabilized cells were incubated with primary antibody anti-4-HNE (Abcam 48506) diluted 1/200 in PBS buffer containing 5% BSA overnight at 4°C. The next day, cells were washed 3x with PBS buffer containing 1% BSA and incubated with the secondary antibody (Alexa Fluor 647, ThermoFisher Scientific) diluted 1/1000 in DPBS buffer containing 1% BSA for 45 min at 37°C. After the final wash with PBS buffer containing 1% BSA, the cover slips were mounted on the glass slides using a mounting medium (ProLong Gold Antifade Reagent).

2.9. Flow cytometry measurements

Transfection efficiency, pH measurements and cell viability were performed with a CyFlow flow cytometer (Partec/Sysmex) equipped with a Flomax software. For the measurement of transfection efficiency, Citrine was excited at 488 nm and detected with a 536/40 nm BP filter, mTurquoise was excited at 405 nm and detected with a 455/50 nm BP filter, and m Cherry was excited at 561 nm and detected with a 610/30 nm BP filter.

For pH measurements, SNARF-1 was excited at 488 nm. The fluorescence of its protonated form was detected with a 590/50 nm BP filter and its deprotonated form with a 675/22 nm BP filter. By calculating a fluorescence intensity ratio of these two forms and using a calibration curve of SNARF-1, final intracellular pH was determined using FlowJo software.

For cell viability, the apoptosis was examined using Annexin-V APC, which was excited at 635 nm and detected with a 675 nm BP.

2.10. Confocal microscopy

For confocal microscopy imaging, cells were seeded on µ-Slide 8 well glass bottom chamber IBIDI and observed in DPBS. Images were acquired with an inverted Leica TCS SP8X microscope using a 63x oil immersion objective (NA 1.4) and a white laser.

2.11. Fluorescence Lifetime Imaging Microscopy (FLIM)

For FLIM experiments, cells were seeded on glass cover slips (⌀ 25mm) in 6-well plates (Greiner Bio-One) in density 0.2 x 10^6/mL. They were transfected 24 h prior to experiment. Transfected cells were studied in PBS at 37°C for 2 h maximum in an Attofluor cell chamber (Thermo Fisher Scientific).

Time resolved laser scanning TCSPC microscopy was performed on a custom-made microscope as described previously [12]. The setup is based on a TE2000 microscope with a 60x, 1.2NA water immersion objective (Nikon). The epifluorescence pathway is equipped with an Hg lamp, a set of filter cubes for the different FPs and a CCD camera (ORCA-AG, Hamamatsu Photonics). The TCSPC path is equipped with pulsed laser diodes (440 nm for CFPs, PicoQuant) driven by a PDL800 driver (20 MHz, PicoQuant). The C1 scanning head (Nikon) probes a 100 x 100 µm maximum field of view. To select the FP fluorescence, dichroic mirrors (DM) and filter sets were used before the detection by an MCP-PMT detector (Hamamatsu Photonics). The signals were amplified by a fast pulse pre-amplifier (Phillips Scientific) before reaching the PicoHarp300 TCSPC module (PicoQuant). Counting rates were routinely between 50 000 and 100 000 cts/s.

The lifetime of a fluorophore is independent of its concentration and a precision of a few percent on lifetime is common [13,14,15]. The TCSPC fluorescence decay of all collected pixels in the selected ROIs was computed using the SymPhoTime software (PicoQuant). As donor, we used fluorescent proteins Aquamarine or mTurquoise, whose fluorescence decay can be fitted with a mono-exponential fit function:

$$I(t) = I_0\, e^{-\frac{t}{\tau_D}} + C \qquad \textit{(Equation 1)}$$

where I_0 is the fluorescence intensity at t = 0, τ_D is the fluorescence lifetime of a donor alone, and C is the constant background.

During the FRET experiment, donor and acceptors are co-expressed in cells. Some donors interact with acceptors, but some may not have any FRET partner. This situation leads to a fluorescence decay fitted with a bi-exponential function:

$$I(t) = \alpha_{long}\, I_0\, e^{-\frac{t}{\tau_{long}}} + \alpha_{short}\, I_0\, e^{-\frac{t}{\tau_{short}}} + C \qquad \textit{(Equation 2)}$$

where α_{long} and α_{short} are the proportions of a long (τ_{long}) and a short (τ_{short}) lifetime components respectively (SI of [16]).

We calculated $< \tau_{\text{DA}} >$, the average lifetime of the donor in presence of the acceptor, as:

$$< \tau_{DA} > = \alpha_{long}\, \tau_{long} + \alpha_{short}\, \tau_{short} \qquad \textit{(Equation 3)}$$

The apparent FRET efficiency (E_{app}) was calculated using $< \tau_{\text{DA}} >$ and τ_{D}:

$$E_{app}\,(\%) = 1 - \frac{<\tau_{DA}>}{\tau_D} \times 100 \qquad \textit{(Equation 4)}$$

The plotting of E_{app} against $[A]/[D]$ required the calibration of fluorescence intensities measured in both donor and acceptor channel in the same ROI used to compute the fluorescence decays. The ratio of fluorescence intensities, $I(A)/I(D)$, was transformed in the concentration ratio of fluorescent proteins, $[A]/[D]$, using a custom calibration procedure of the microscopy setup (see SI, Figure S9). Image treatment was performed in Image J (NIH, USA).

2.12. Statistical Analysis

Data in graphs are represented as means of at least three independent experiments ±SEM. For pH measurements, the significance was tested with Student's test, for FRET-FLIM experiments with one-way ANOVA. The statistical analysis was performed using R version 3.5.3.

3. RESULTS

3.1 Trimera enables the active state of the NADPH oxidase in cells

We expressed either the separated cytosolic subunits, p67^{phox}, p47^{phox} and p40^{phox}, each labeled with a fluorescent protein (FP) or the Citrine-Trimera [6], [7] in COSNOX cells, COS-7 cells stably expressing p22^{phox} and gp91^{phox} subunits [8]. The COSNOX cells contain endogenous Rac1 [17]. The ROS production was detected by the L-012/Horseradish Peroxidase (HRP) luminometry assay (Figure 2). The COSNOX cells expressing the separated subunits were stimulated by phorbol ester, PMA. The PMA is a soluble stimulus, which launches phosphorylation of NOX subunits through activation of protein kinase C. As expected with this activation process, the luminescence signal raised slowly and reached a plateau at around 30 min. We also observed that p40^{phox} was not necessary to induce a strong NADPH oxidase activity and the presence of p40^{phox} actually decreased the ROS production almost twice (Figure 2A and C). This observation supports the hypothesis of p40^{phox} being a negative regulator in a PMA-stimulated situation [18], [19]. In COSNOX cells expressing the Trimera, a strong signal is detected immediately after the addition of the L-012/HRP mixture without any chemical stimulation. The signal raised quickly for a few minutes, likely the time necessary to reach the steady state of the detection reaction, and then reached a plateau (Figure 2B). This plateau can be seen as a "snapshot" in the time period during which the ROS are produced continually in presence of the Trimera. These results confirmed the previous observations of the constitutive NADPH oxidase activity elicited by the Trimera and measured with the cytochrome *c* assay by Masoud *et al.* [6]. Addition of PMA to the COSNOX cells expressing only Trimera did not influence the ROS production (data not shown). The addition of DPI, a NADPH oxidase inhibitor, at the end of the measurement caused an immediate and steep drop in the luminescence signal showing an efficient inhibition of the oxidase activity (Figure S3). In order to evaluate if the separate cytosolic subunits may influence the constitutive activity of the Trimera-induced NADPH oxidase, either p47^{phox} and p67^{phox} or p40^{phox} were co-expressed with the Trimera in COSNOX cells (Figure 2B). After 15 min of activation by PMA, the ROS production levels were very similar to the level reached by cells expressing only the Trimera. Comparison of the total ROS production in a 30 min measurement showed no significant difference between these conditions (Figure 2D). mCherryp40^{phox} alone has no effect on the Trimera ROS production. For the separated cytosolic subunits, p47^{phox}mCherry and p67^{phox}mTurquoise, activated by PMA, we can assume that once the Trimera is expressed in cells, it occupies most of gp91^{phox}/p22^{phox} "docking sites" in the membrane, hindering the formation of additional active complexes. Moreover, the small G protein, Rac is known to play a central role in the recruitment of the cytosolic subunits to the membrane-bound gp91^{phox}/p22^{phox} during the activation phase of the NADPH oxidase. In the Trimera, Rac1 bears the mutation Q61L leading to Rac1 being fully in its active form bound to GTP (dominant-positive). We compared the ROS production induced by this Trimera with Trimera containing the wild type version of Rac1 (Rac1 61Q or WT) and Trimera containing the dominant-negative version, Rac1 T17N that prevents the formation of the active GTP bound form [8] (Figure 2E). Expression of Rac1 Q61L or its wild type version in COSNOX cells lead to very similar levels of ROS production, whereas the dominant-negative mutant leads to less ROS production. Rac1 bound to GTP is the active form that allows its binding to effectors including p67^{phox}. In the Trimera, Rac1 and p67^{phox} are already bound. This binding and its structural consequences may partially compensate the lack of activation of Rac1 in the T17N version. Accordingly, we observed that the fusion allows a moderate ROS production. On the other hand, our observations suggest, that the fraction of active Rac1 in the Trimera equipped with the WT version is sufficient to induce a ROS production comparable to the Trimera Rac1 Q61L where 100% of Rac1 is active. This could be due to the relative expression levels of each partners in the living cells. Indeed, the transient expression of FP-Trimera is likely higher than the stable expression of gp91^{phox}/p22^{phox} in COSNOX cells. As a consequence, only a fraction of FP-Trimera may be required to "cover" the cytosolic side of all p91^{phox}/p22^{phox} subunits. Saturation of NOX2/p22^{phox} binding sites by overexpressed FP-trimera may also explain the limited access of p47^{phox} and p67^{phox} when co-expressed with Trimera. This saturation thus leads to comparable ROS production levels observed with or without co-expression of p47^{phox} and p67^{phox} in Figure 2D. Therefore, in a next step, we were wondering if the Trimera requires the presence of gp91^{phox} or p22^{phox} and an active Rac1 to locate at the plasma membrane.

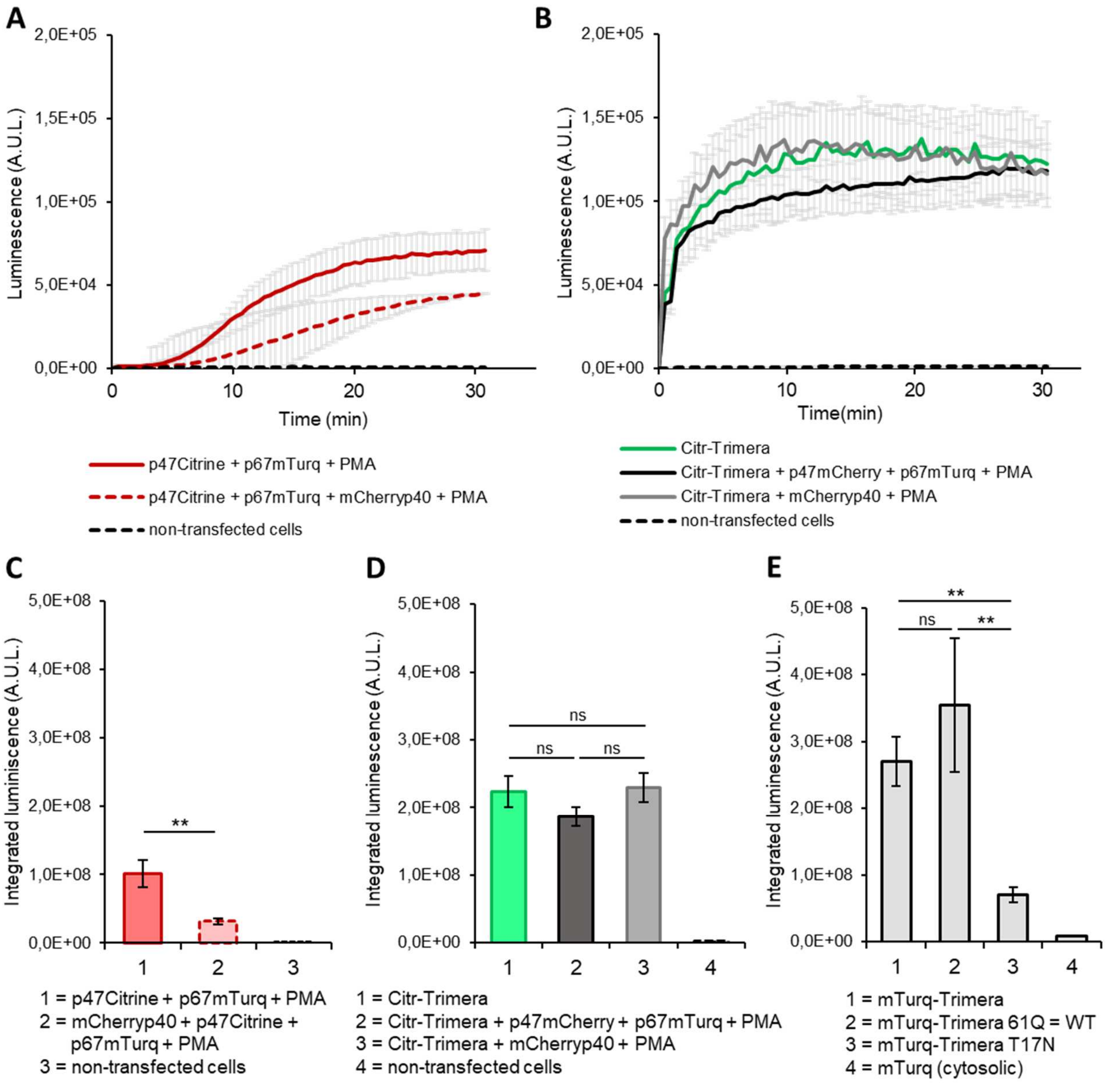

Figure 2. Constitutive ROS production elicited by the Trimera A: *Effect of p40^{phox} on the ROS production in COSNOX cells transfected with individual NOX subunits. Representative luminometry experiment (duplicates, error bars show SD).* ***B:*** *Effect of the individual NADPH oxidase subunits on the Trimera-elicited ROS production in COSNOX cells. Representative luminometry experiment (duplicates, error bars show SD). Activation by 1 µM PMA and non-transfected COSNOX cells were used as positive and negative controls respectively. Integrated luminescence signals (total ROS production) for 30 min of measurement for the panel A is shown in* ***C*** *(error bars show SEM for 4 independent experiments and statistical analysis was performed by t-test; ** means $p < 0.01$), for the panel B shown in* ***D*** *(error bars show SEM for 3 independent experiments and statistical analysis was performed by one-way ANOVA), and for Trimeras bearing three variants of Rac1 shown in* ***E*** *(error bars show SEM for 3 independent experiments and statistical analysis was performed by one-way ANOVA; ** means $p < 0.01$). In* ***E****, mTurq-Trimera contains the same Trimera as it is in the Citr-Trimera construct (with the Rac1Q61L), mTurq-Trimera*

61Q = WT stands for the construct containing the Trimera with the wild type Rac1. mTurq-Trimera T17N stands for the construct containing the Trimera with the Rac1T17N (dominant-negative).

3.2 Trimera localizes in the plasma membrane independently of gp91^{phox} and p22^{phox}

We already observed the location of the Trimera at the plasma membrane of COSNOX cells [6]. We now compare the localization of the fusion protein FP-Trimera (FP being either Citrine or mTurquoise) in three cell lines, COS-7, COS^{p22} and COSNOX (Figure 3A) and with three variants of Rac1 in COSNOX (Figure 3B); COS-7 cells do not contain any of the NADPH oxidase subunits except Rac, COS^{p22} cells stably express the p22^{phox} subunit and COSNOX were described in previous paragraph. Using confocal microscopy, we observed that whatever the Trimera and the transfected cell types, their localizations were predominantly at the plasma membrane. These results suggest that the presence of neither gp91^{phox} nor p22^{phox} is necessary for the Trimera binding to the membrane. This also suggest that an active Rac1 is not required for the anchoring of the Trimera at the membrane as we did not observe a clear change of phenotype with Rac1 T17N. The fluorescent and bright aggregates found in cytosol and nucleus may be due to the binding of a fraction of Rac1 to the nucleocytoplasmic shuttling protein SmgGDS protein as it was already observed [20], [21]. Moreover, Rac 1 bears a nuclear localization signal in its polybasic domain and can be imported via Karyopherin a2 in the nucleus [53]. This may be the case for the Trimera as well.

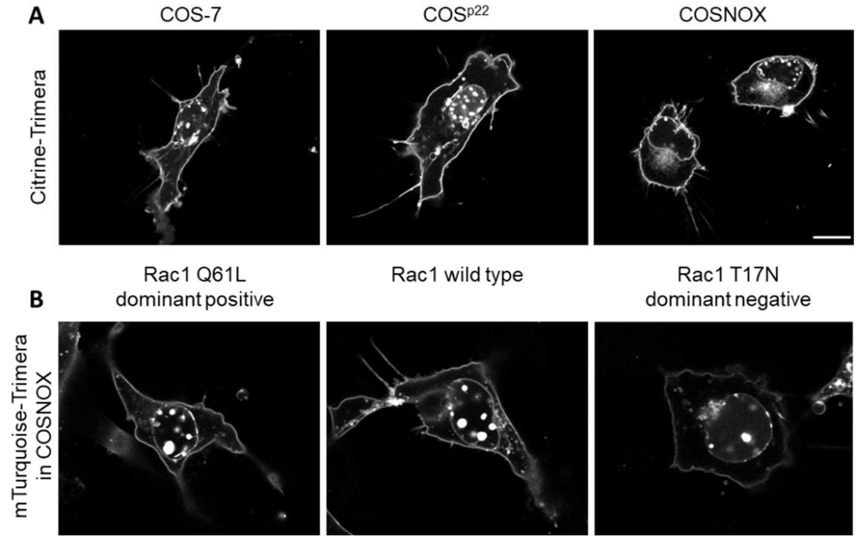

Figure 3. Trimera localization in cells. *Confocal images of* ***A.*** *Citrine-Trimera in COS-7, COS^{p22} and in COSNOX cells. Same scale bar for all images in the row, 10 µm.* ***B.*** *mTurquoise-Trimera Rac1 Q61L (dominant-positive), Rac1 61Q (wild type) and Rac1 17N 61Q (dominant-negative) in COSNOX cells. Same scale bar for all images, 10 µm.*

3.3 Continuous NADPH oxidase activity causes an overall decrease of intracellular pH

When Trimera protein is expressed in COSNOX cells, it binds to the plasma membrane, joining the two membrane subunits and turning the NADPH oxidase into the active state. The continuous NADPH oxidase activity leads not only to the $O_2^{\bullet -}$ overproduction outside of the cell but also to a massive release of H^+ in the cytosol upon NADPH oxidation into $NADP^+$. In this paragraph, we focus on the pH variations induced by the continuous NADPH oxidase activity.

We measured the intracellular pH in COSNOX cells with the ratiometric fluorescent SNARF-1 probe, whose fluorescence is pH sensitive, under different conditions using flow cytometry. In these experiments, the Trimera was labelled with mTurquoise (mTurq). Indeed, mTurquoise's fluorescence is compatible with the concomitant observation of pH with SNARF-1 without spectral bleed-through. The non-transfected COSNOX was chosen as the reference with an average pH value of 7.2 (Figure 4A). Control cells expressing mTurquoise alkalinized slightly, but not in a significant way. In cells expressing mTurq-Trimera, the pH value decreased significantly by 0.2 pH unit. When we added DPI to the cells expressing mTurq-Trimera, pH was restored to its initial value after 15 min with no further evolution after 45 min (Figure 4A). We controlled that we did not observe any pH recovery in cells expressing mTurq-Trimera treated with DMSO, the DPI solvent. For the negative control, we expressed mTurquoise or mTurq-Trimera in COS-7 cells and we did not detect any decrease of the intracellular pH (Figure 4B), the initial pH value for COS-7 cells being close to 7.4. These findings confirm that NADPH oxidase activity is indeed the source of the cytosol acidification.

The observed acidification raised the question of the pH regulation in the COS-7 cells used in the study. Indeed, on the contrary to professional phagocytes, in which the pH variations due to the NADPH oxidase activity are counter balanced by proton channels, the COS-7 cells do not have such channels [22]. Nevertheless, COS-7 cells express a Na^+/H^+ exchanger and we explored its potential role in the cellular pH equilibration. These experiments required a buffer devoid of Na^+, to avoid any contribution of the Na^+/H^+ exchanger to the pH equilibration. The cells expressing mTurquoise-Trimera were thus incubated a N-Methyl-D-glucamine buffer (NMDG buffer, see Material and Methods) for 1h just before the pH measurement. As shown in Figure 4A, cells in NMDG buffer acidified markedly, with their cytosolic pH decreasing by 0.5 pH unit. These data indicate that the Na^+/H^+ exchanger extrudes the H^+ generated in the cytosol by NADPH oxidase and is therefore required to balance pH fluctuations.

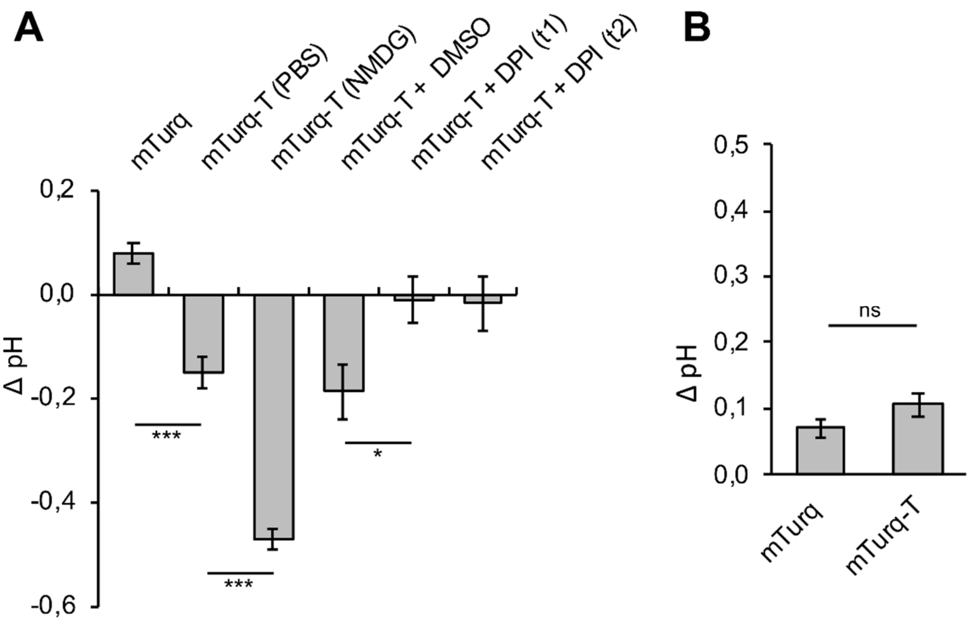

Figure 4. Continuous NADPH oxidase activity causes acidification of the intracellular pH in COSNOX cells. A: *Comparison of ΔpH in COSNOX cells 24 h after the transfection by mTurquoise-Trimera or mTurquoise. ΔpH was calculated always against the intracellular pH of non-transfected COSNOX cells (average pH value of 7.16). The DPI was added 15 min (t1) and 45 min (t2) before pH measurement. Means and errors bars (SEM) for 5 independent experiments. Statistical analysis performed by t-test (***p<0.001).* ***B:*** *Negative control. Comparison of ΔpH in COS-7 cells 24 h after the transfection mTurquoise-Trimera or mTurquoise. Errors bars show SEM for 3 independent experiments. Statistical analysis performed by t-test.*

3.4 Continuous NADPH oxidase activity triggers apoptosis

Furthermore, the continuous activation of the NADPH oxidase leads to a massive $O_2^{\bullet-}$ overproduction. Part of the cocktail of ROS produced, may cause oxidative stress, damage proteins, nucleic acids, lipids, membranes and organelles and finally affect cell survival [23].

We first evaluate the influence of this massive production on cell viability. These experiments have been performed using Annexin V as apoptosis marker and the cells were analyzed by flow cytometry (Figure 5). We investigated the percentage of apoptotic cells within the COSNOX cell population expressing Citrine-Trimera 24 h after transfection. As negative controls, we used COSNOX cells expressing Citrine or COS-7 expressing Citrine-Trimera. To compare highly fluorescent cells in the Citrine channel with cells showing lower fluorescence intensities, we defined two zones in the quadrant Q2 of the dot plots, Q2' and Q2'' The percentage of apoptotic cells (quadrant Q2) among Citrine positive cells (quadrant Q2 + Q3) were calculated from the dot plots.

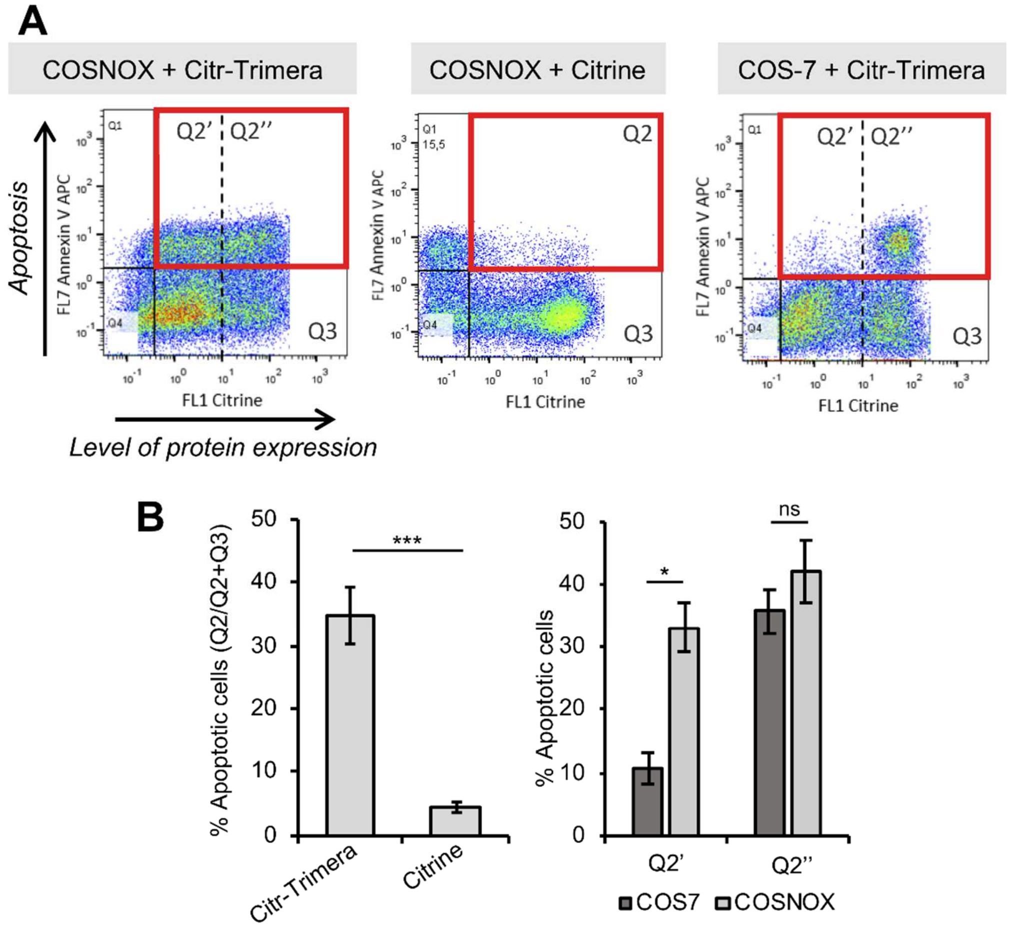

Figure 5. Influence of the continuous NADPH oxidase activity on cell viability. A: *Apoptosis in COSNOX/COS-7 cells 24 h after the transfection with Citrine-Trimera or Citrine. The dot plots show representative experimental data. The quadrant Q2 (in red) contains cells expressing the protein of interest and being apoptotic as well. Q2' contains cells with moderate expression level of Citrine-Trimera. Q2" contains cells with high expression level of Citrine-Trimera.* ***B:*** *Left: Mean % of apoptotic cells in Q2 in COSNOX cells. Right: Comparison of mean % of apoptotic cells in Q2' and Q2" for COSNOX or COS-7 cells transfected with Citrine-Trimera. Errors bars show SEM for 4 independent experiments. Statistical analysis performed by t-test and one-way ANOVA test followed by a Tukey's Multiple Comparison Test (*** means $p < 0.001$, * means $p < 0.05$).*

The percentage of apoptotic cells was significantly increased in the cells expressing Citrine-Trimera compared to cells expressing Citrine only (Figure 5A and 5B left). COS-7 cells do not contain any of the membrane subunits of the NADPH oxidase and do not present any NADPH oxidase activity in presence of Trimera [6]. In those cells few apoptotic cells were detected in Q2', whereas numerous apoptotic cells were detected in Q2'', the zone of high Citrine-Trimera expression (Figure 5A, at the very right). By contrast, in COSNOX cells a significantly increased level of apoptotic cells was observed in Q2' showing the effect of ROS produced by active NADPH oxidase (Figure 5B right). The percentage of apoptosis reached even higher levels in the Q2'' zone of COSNOX cells expressing Citrine-Trimera as compared to COS-7 cells (Figure 5B right). Taken together, these results indicate that long-term continuous NADPH oxidase activity and subsequent oxidative stress induces apoptosis in cells.

3.5. Increased levels of ROS induce lipid peroxidation of plasma membrane

In this next step, we were wondering if the elevated levels of oxidative stress could induce lipid peroxidation of the plasma membrane. Indeed, the continuous NADPH oxidase activity elicited by the Trimera located at the plasma membrane decreased the cell viability by causing apoptosis that could be triggered by lipid peroxidation [24]. The peroxidation may alter lipid asymmetry and lipid polarity, which affects membrane surface, membrane proteins and enzymes [25]. As a consequence, changes in the membrane thickness, membrane fluidity, and membrane permeability may appear and disrupt normal cell metabolism [26].

First, we opted for an immunostaining strategy to detect 4-hydroxynonenal (4-HNE), one of the products of lipid peroxidation, which is commonly detected as a marker of the process [24], [27], [28]. Second, we used a super-resolution infrared (IR) technique derived from an atomic force microscopy (AFM), called AFM-IR [29] in order to evaluate, at the nanometer scale, the morphological and chemical modifications that occur in the plasma membrane.

To detect 4-HNE, we used a primary antibody anti-4-HNE in combination with a secondary IgG antibody labeled by Alexa Fluor 647. Fluorescence intensity of Alexa Fluor 647, which corresponded to the amount of 4-HNE in cells, was analyzed by confocal microscopy (Figure S4). The positive control - COSNOX cells treated by the external addition of H_2O_2 showed significantly increased fluorescence intensity in comparison to all other conditions. However, there was no significant difference in 4-HNE levels between COSNOX cells transfected with Citrine-Trimera or Citrine alone compared to the non-transfected cells. Thus, the continuous

NADPH oxidase activity does not engender distinctly increased levels of 4-HNE in COSNOX cells.

The second approach to search for morphological and chemical modifications in the plasma membrane induced by the continuous NADPH oxidase activity was IR imaging methodologies. Biomolecules, such as nucleic acids, proteins, lipids, and carbohydrates can be directly probed without any labeling as they possess their own typical vibrational fingerprints in the mid-IR region [30, 31] (Figure S5B).

Furthermore, after lipid peroxidation, a huge variety of products like alcohols, ketones, aldehydes, and ethers might be found [32]. Two new chemical features, that might be observed, are the appearance of hydroperoxy (C-O-OH) or carbonyl (C=O) groups in diverse oxidized phospholipid products. The IR absorption of the C=O bond is extremely sensitive to its environment and to the other chemical groups present in its vicinity. In the literature, a band in the region 1755–1720 cm^{-1} (centered at 1740 cm^{-1}) is generally assigned to the C=O bond in functional groups like esters, aldehydes, ketones and was described as a signature of the end products of lipid peroxidation in various biological samples [33, 34, 35].

First, we evaluated the effect of massive NADPH oxidase activity using classical IR imaging, which probes the area of 20 μm x 20 μm, and thus provides IR absorption spectra of the entire cell without subcellular spatial resolution. We compared individually the IR signature of COSNOX cells expressing or not the Citrine-Trimera in the same field of view. Their IR absorption in the region 1755–1720 cm^{-1} was identical (Figure S6). If lipid peroxidation processes occurred at the subcellular level as supposed, the inherent low lateral resolution of the IR imaging technique (being in the order of the wavelength between *2,5-10 μm* for mid-infrared range), would impede their detection. Therefore, we decided to investigate COSNOX and COS-7 cells expressing or not the Citrine-Trimera using an innovative IR nano-spectroscopy technique called AFM-IR (Figure S5). This method is a hybrid technique combining the high spatial resolution offered by an atomic force microscope, AFM, and the chemical analysis offered by InfraRed (IR) spectroscopy. This method allows to acquire simultaneously (i) AFM images (topography of the surface – morphological analysis) and (ii) IR chemical maps at a specific wavenumber (location of specific compounds within the cell). Moreover, it also gives a possibility to acquire very local IR absorption spectra at a chosen region of interest (ROI) of the sample. Those local IR spectra allow to determine chemical composition of the surface sample, which is just under the AFM tip, with a lateral resolution in the range of *~ 20 nm*.

Non-transfected COXNOX cells or COS7 cells transfected with Citrine-Trimera were chosen as the negative control (Figure 6A and D). COSNOX cells incubated with H_2O_2 corresponded to the positive control (Figure 6E and E'). The fluorescent cells expressing Citrine-Trimera or Citrine were first identified by wide-field fluorescence microscopy before the analysis by AFM-IR. For each condition, we acquired a topography showing the surface of the cells (Figure 6, left columns). Then a zoomed ROI (100 - 200 µm²) in the membrane, was chosen to collect the chemical information at two specific wavenumbers. The first IR maps at 1660 cm^{-1} is representative of the total protein content in the ROI and will serve at a reference whereas the second one, at 1740 cm^{-1}, is the signature of lipids peroxidation (Figure S7 for the IR map at 1740 cm^{-1}).

The control cells exhibited a homogenous distribution of the IR signal for both wavenumbers and a low absorption at 1740 cm^{-1} (Figure S7A and D). This was further illustrated by calculating the ratio between the 1660 cm^{-1} map and the 1740 cm^{-1} map, which allows a direct comparison of the amount of C=O bond in esters, aldehydes, ketones groups to total protein content (Figure 6A and D, blue ratio maps). For both non-transfected COSNOX cells and COS-7 cells transfected with a high amount of the Citrine-Trimera, the ratio map was homogenous with a maximum value of 1740/1660 cm^{-1} below 0,3 (ratio histogram on the right side of the map). In order to confirm this trend locally, full AFM-IR spectra from 1900 to 900 cm^{-1} were acquired at chosen locations of the AFM tip (specified by arrows in Figure 6, corresponding spectra in the very right column). Those spectra represent the mean IR absorption of a *~20 nm* size area. The local IR spectra, for both negative controls, present the strong characteristic IR bands of the protein peptide bond (amide I at 1660 cm^{-1} and amide II at 1540 cm^{-1}) with a low shoulder at 1740 cm^{-1} (oxidized lipids). In addition, the IR absorption is low in the fingerprint region of the spectra corresponding mainly (i) to other bonds in proteins and lipids (for example C-H bending at 1480-1350 cm^{-1}) and (ii) to the characteristic bands for carbohydrates and phosphates (Figure 6A and D).

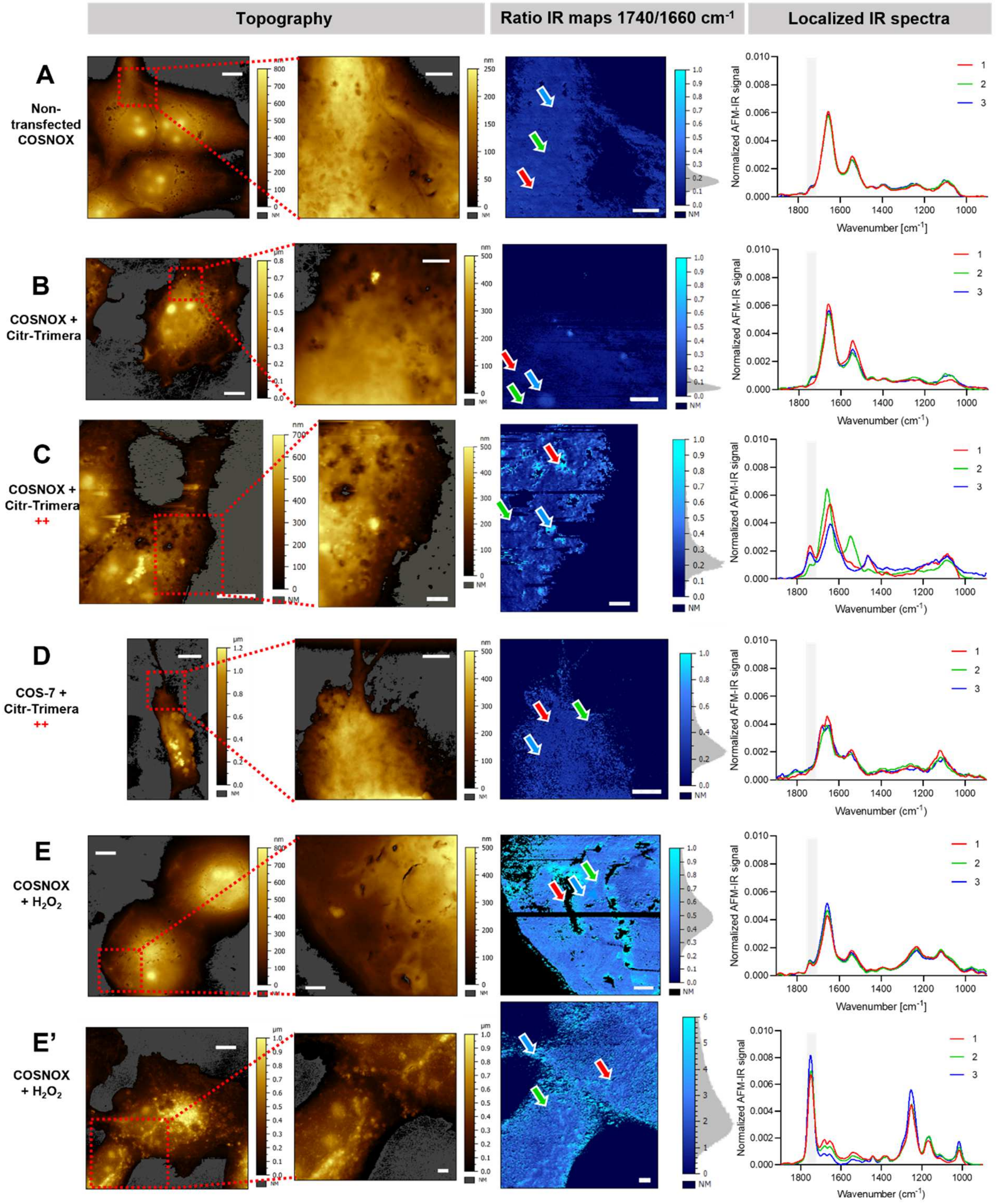

Figure 6. AFM-IR analysis: Detection of chemical modification in cell plasma membrane. *The 'Topography' column shows height images of the analyzed cells and of a zoomed area in the cell plasma membrane (red dashed square). Column 'Ratio IR maps 1740/1660 cm^{-1}' corresponds to the calculated ratio of two IR maps of the zoomed area, one acquired at 1740 cm^{-1} and one at 1660 cm^{-1} (ratio histogram on the right side of the map).* ***A:*** *Non-transfected and non-treated COSNOX cells.* ***B:*** *COSNOX cells transfected with an amount of the Citrine-Trimera DNA normally used for transfections.* ***C:*** *COSNOX cells transfected with a high amount of the Citrine-Trimera DNA (three times more than for the normal transfection as in B).* ***D:*** *COS7*

cells transfected with a high amount of the Citrine-Trimera DNA. ***E + E':*** *COSNOX cells treated with 200 µM H_2O_2 overnight. The last column shows three representative hyper-local spectra. Colored arrows on the ratio image (with corresponding colors) show the location of these spectra. Spectra were normalized to the area under the curve. The spectral region concerning the lipid peroxidation-related signal (1740-1755 cm^{-1}) is highlighted in grey. The data and the images were processed using Orange and MountainMaps software respectively. Scale bars 10 µm for large topographies, 2.5 µm for the zoomed regions, NM = non measured (background pixels). At least 7 cells from 2 independent experiments per condition were analyzed. Representative cells for each condition are shown.*

As we cannot control the transient expression level of proteins, we transfected the COSNOX cells with two different quantities of plasmid DNA to induce very different expression levels of the Citrine-Trimera (noted Citrine-Trimera and Citr-Trimera++ in Figure 6). A pattern similar to non-transfected cells is observed for COSNOX cells expressing low level of Citrine-Trimera (Figure 6B). Nevertheless, at some locations, a slight band at 1740 cm^{-1} appeared associated with a modest increase of absorption in the low fingerprint region (Figure 6B, arrows *2 and 3*). These features are much more pronounced when the level of Citrine-Trimera increased (Figure 6C) and hotspots of absorption appeared on the ratio map. Although the maximum value of the ratio increased only sparsely on the histogram represented along the map. The light-blue hotspots in COSNOX cells expressing Citrine-Trimera corresponded to strong and localized absorption at 1740 cm^{-1} (Figure 6C, spectra corresponding to arrows, Figure S8 for more examples).

For the positive control cells treated with H_2O_2, the peroxidized-species to protein ratio increased significantly above 0.3 and up to 6 in certain cells (figure 6 E and E') but the absorption at 1740 cm^{-1} seemed to be more homogenously distributed with smaller, and diffuse hotspots compared to the COSNOX cells expressing a high amount of Trimera.

The spectra Figure 6 show that the strong band at 1740 cm^{-1} is associated generally with four well-defined bands in the fingerprint region at 1260-1250 cm^{-1}, 1171-1160 cm^{-1}, 1110-1100 cm^{-1} and 1020-1010 cm^{-1}. Especially, the strong absorption band observed at 1260 cm^{-1} could be assigned to the C-O stretching (mixed with the O-H in plane bending) of lipid hydroperoxides [24]. For the positive control, COSNOX cells treated with H_2O_2, we observed some heterogeneity between cells. In some cells, a moderate signal at 1740 cm^{-1} was detected (Figure 6E), whereas in others a strong signal at 1740 cm^{-1} associated with the new bands in the fingerprint region was observed (Figure 6E'). We assign this heterogeneity to biological variations among individual cells in terms of the antioxidant enzymes that could eliminate H_2O_2 in cells.

The local spectra indicated that the IR bands at 1740 cm^{-1} as well as at 1260-1250 cm^{-1}, 1171-1160 cm^{-1}, 1110-1100 cm^{-1} and 1020-1010 cm^{-1} were also present in the cells exposed to H_2O_2; those bands being likely due to the lipid peroxidation as described in the literature [30]. The relative intensity of those bands is strongly linked to the final mixture of peroxides that may slightly differ from the one obtained in COSNOX cells expressing Citrine-Trimera. The negative controls confirmed that the signal peak at 1740 cm^{-1} was directly related to the expression level of Citrine-Trimera in the COSNOX cells. The comparison of different expression levels of the Trimera protein suggest that the presence of those bands was most probably due to lipid peroxidation caused by intensive NADPH oxidase activity.

This chemical signature of oxidative stress is less specific than the detection of 4-HNE. The immunostaining of 4-HNE detects a single oxidized species, whereas the IR signal at 1740 cm^{-1} may correspond to many different oxidized molecules. The IR signal likely reflects the molecular diversity of the chemical modifications induced by the sustained NADPH oxidase activity. An interesting finding was the localized distribution of the oxidation in hotspots of a few hundreds of nm. This was quite surprising as we rather expected a homogenous ROS production in the cell membrane.

3.6. Trimera forms clusters in the plasma membrane independently of gp91^{phox}

In order to understand the localized oxidative damages observed with the AFM-IR technique, we investigated the Trimera membrane distribution. To this aim, we decided to exploit the Förster Resonance Energy Transfer (FRET) between two fluorophores, a donor, mTurquoise, and an acceptor, mCitrine fused to the Trimera and expressed together (Figure 7A). The fluorescence emission spectrum of mTurquoise overlays the absorption spectrum of mCitrine, so both FPs fulfill the spectral condition for FRET: upon their excitation, the donors, in the excited state, can transfer part of their energy to the acceptors in the ground state, which in turn become fluorescent. The FRET efficiency is highly dependent on geometrical parameters such as the donor/acceptor distance, which must be less than 10 nm (Figure 7A) and on protein topology. Consequently, the FRET efficiency between donors and acceptors fused to the protein of interest and co-expressed in the cells can be used to evaluate the distribution of those proteins at the membranes, where the average spacing depends on their concentration and lateral distribution.

Proteins can be homogeneously and randomly distributed in the membrane, they can form clusters, or they can create a mixed distribution containing clusters and free molecules (Figure 7B, upper row). The organization at the molecular level influences the possibility of FRET to occur: an efficient FRET can be observed if two molecules are close either due to clustering, or due to high concentrations and packing, which bring them close enough even in the absence of microdomains [36], [37]. Consequently, the FRET efficiency varies with the density of labelled proteins in the cell membrane [38].

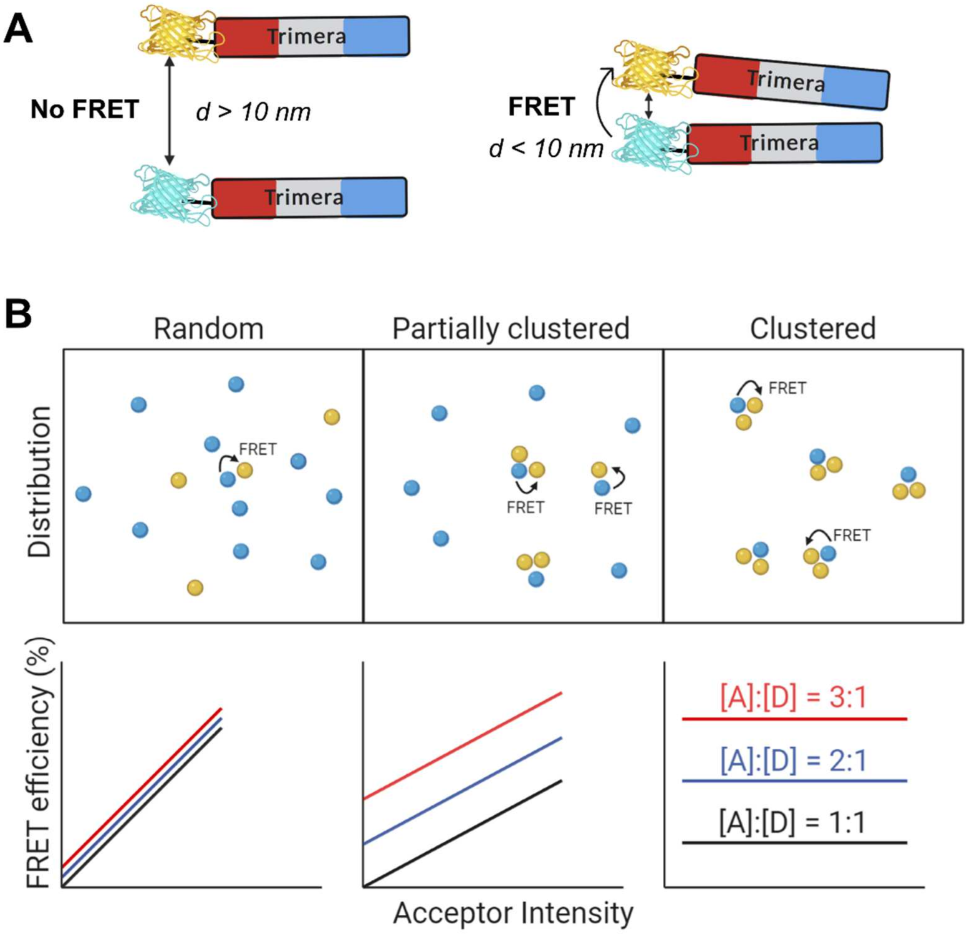

Figure 7. Investigation of protein distribution in membrane of living cells by FRET. A: *In case that Trimera proteins labeled by a donor (mTurquoise) or by an acceptor (mCitrine) are in close proximity, the FRET phenomenon will occur.* ***B:*** *Possible distributions of membrane-bound proteins (top) and associated FRET efficiency curves (bottom). Adapted from* [38]. *In our study, we measured the FRET variations by FLIM.*

In a random distribution, the FRET efficiency increases linearly with the acceptor surface density that is proportional to its fluorescence intensity. By contrast, in case of a clustered distribution, the FRET efficiency will depend on the relative quantity of donors and acceptors in the cluster. If the clusters are small enough or sufficiently diluted, there will be no energy transfer between them. Thus, the FRET efficiency will be independent of the acceptor intensity for given acceptor-to-donor ratios. The intermediate situation concerns a partially clustered distribution. So, monitoring FRET efficiencies as a function of the acceptor fluorescence intensity for different acceptor-to-donor ratios reveals a pattern characteristic for each type of distribution curve (Figure 7B, bottom row) [38].

First, we validated our experimental approach on a model system using myristoylated and palmitoylated (MyrPalm) fluorescent proteins, which are known to clusterize in the plasma membranes (Figure 8A) [36]. We transfected the COS-7 cells simultaneously by MyrPalm-Aquamarine (donor) and MyrPalm-YFPA206K (acceptor). The DNA concentration of the MyrPalm-YFPA206K used for transfections was modulated in order to expand the range of acceptor fluorescence intensities and various [A]/[D] ratios. For each cell, the donor fluorescence lifetimes and donor and acceptor fluorescence intensities were measured successively. The apparent FRET efficiency (E_{app}) was evaluated from the donor lifetimes using Equation 3 (see Material and Methods) and the relative acceptor-to-donor concentration ([A]/[D]) was deduced form the intensities thanks to the custom calibration (see SI). Cells were classified in three categories depending on the [A]/[D] ratio: 0-1, 1-3 and > 3.

Our results show different levels of FRET efficiency for each relative concentration [A]/[D] ratio. Those efficiencies are predominantly independent of the acceptor fluorescence intensity, the slopes of the fitting curves being very low (Figure 8A, left). To modulate the distribution of MyrPalm proteins in the membrane, the cells were treated with 10 mM 5-methyl-β-cyclodextrin (MβCD), a treatment known to disrupt lipid rafts and caveolae by depletion of cholesterol [39]. The slopes of fitting curves drastically increased, they became three times larger (Figure 8A, right and 8C), indicating the alteration of protein distribution and a decrease in the level of clustering as expected for MyrPalm-FPs proteins that are known to cluster in lipid rafts. Thus, our experimental workflow was suitable for the investigation of protein clustering.

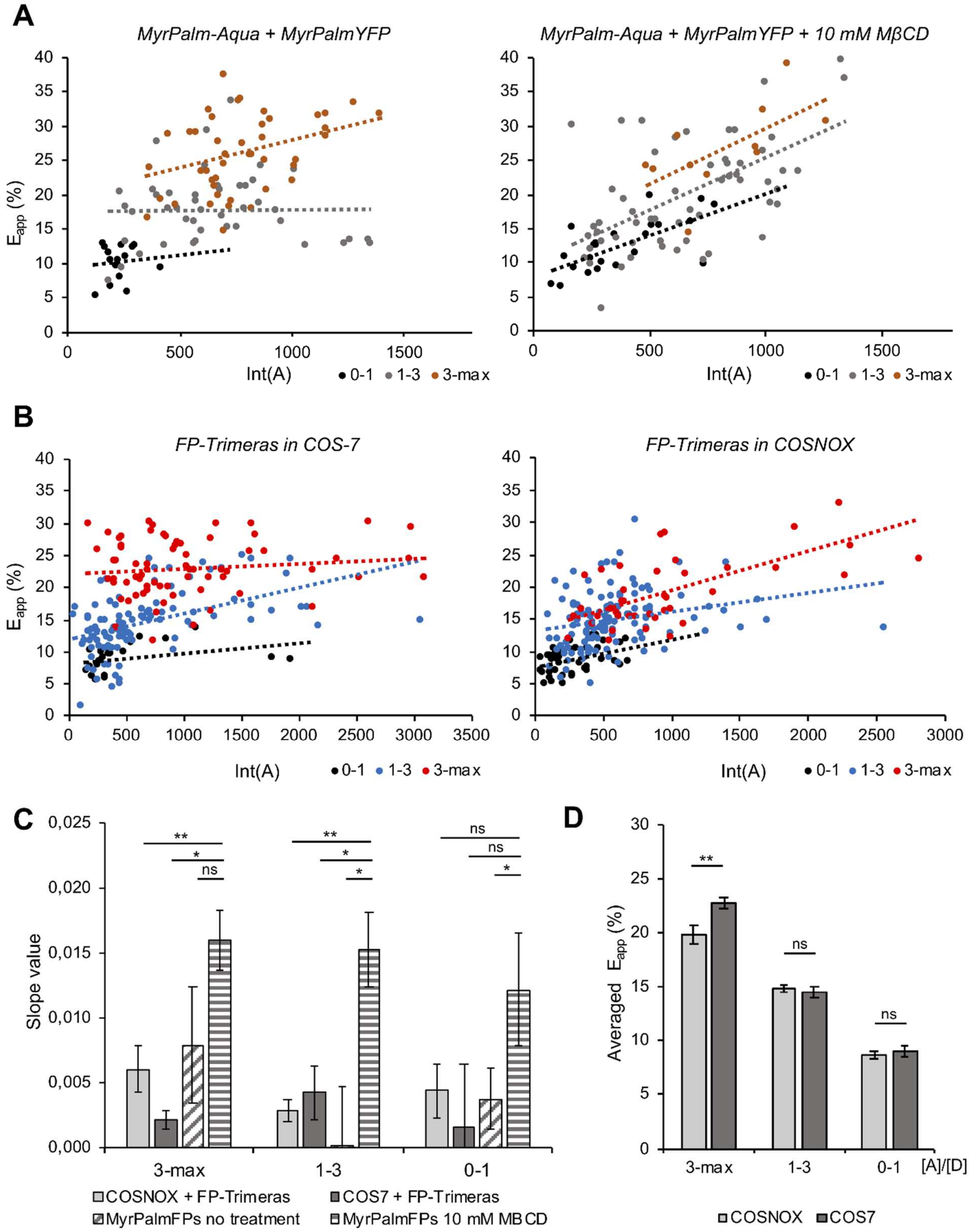

Figure 8. Distribution of MyrPalm proteins (model system) and Trimera proteins in living cells monitored by FRET-FLIM. *Graphs show FRET efficiency (E_{app}) in function of the acceptor intensity. Cells were classed in three different [A]/[D] ratios (different colors).* ***A:*** *COSNOX cells transfected by MyrPalm-Aquamarine and MyrPalm-*

YFPA206K were analyzed without any special treatment (left) or they were treated with 10 mM MβCD (right). ***B:*** *mCitrine-Trimera and mTurquoise-Trimera were expressed in COS-7 cells (left) or in COSNOX cells (right).* ***C:*** *Comparison of slopes of fitting curves for FP-Trimeras and MyrPalm-FPs FRET-FLIM experiments.* ***D:*** *Comparison of averaged E_{app} between COSNOX and COS-7 cells for selected range of the acceptor intensity: Int(A) = 500-900. Error bars show SEM for n = 3 experiments. Statistical analysis performed by one-way ANOVA followed by a Tukey's Multiple Comparison Test (** means $p < 0.01$).*

Therefore, we used the same analytical workflow to investigate the FP-labeled Trimera distribution in the plasma membrane. mTurquoise-Trimera and mCitrine-Trimera were expressed in COS-7 or COSNOX cells in order to evaluate a possible implication of the membrane subunits (gp91^{phox} and p22^{phox}) in Trimera spatial organization at a subcellular level. Different ratios of [A]/[D] were generated as previously for MyrPalm-FPs. During the data treatment, the cells were classified into three categories depending on the [A]/[D] ratio. The E_{app} for each category was plotted against the acceptor fluorescence intensity as shown in Figure 8B.

The slopes of the fitting curves obtained for both the FP-Trimeras in COS-7 or COSNOX cells were close to those of non-treated MyrPalmFP proteins in each [A]/[D] category (Figure 8C). These findings suggest a mainly clustered distribution of the FP-Trimera in both cell lines.

To assess if COS-7 and COSNOX cell lines show genuinely the same distribution in this experiment, averaged E_{app} for every [A]/[D] ratio (Figure 8D) was compared. It increased systematically with the growing [A]/[D] ratio and the highest E_{app} values (~ 20%) were found for the category 3-max of [A]/[D]. This is also seen via the relative position of the linear fits of the experimental dots: the red fitting line for the highest ratio is above the blue and the black one. This is likely a consequence of the increase of the intra-cluster FRET efficiency with the [A]/[D] ratio as it is illustrated in Figure 7B (arrows): statistically, within a cluster, the number of potential FRET acceptors increases in the vicinity of each donor. For the category 3-max of the [A]/[D] ratio, we observed a significant difference in the average E_{app} between COS-7 and COSNOX; average E_{app} values being higher for COS-7 cells (Figure 8D). Since we detected the ROS production in COSNOX cells expressing Trimera, the latter has to interact directly with gp91^{phox}/p22^{phox} complexes. We can speculate that the presence of gp91^{phox}/p22^{phox} in the Trimera clusters in COSNOX cells may impose topological constraints on the relative A/D distance for example. These constraints have certainly consequences on the intra-cluster FRET efficiency, as they could be observed only for the highest [A]/[D] ratio (3-max, Figure 8D), when the contribution of the intra-cluster FRET is likely predominant. The specificity of the Trimeragp91^{phox} interaction requires further experimental investigations, which might also help to explain the role of gp91^{phox} in the clustering process.

4. DISCUSSION

4.1. Membrane targeting and constitutive ROS production

We showed that Trimera localizes to the plasma membrane independently of gp91^{phox}/p22^{phox} subunits and this result raises the question of the membrane targeting of the Trimera. The membrane targeting of the small G-protein Rac1 is ensured by the exposition of its polybasic region (PBR) in a GTP-bound form and by the attachment of a lipid anchor to its C-terminus [40]. GDP-bound Rac1 binds to RhoGDI, which prevents its attachment to the membrane. In the Trimera sequence, Rac1Q61L is present at the C-terminus (Figure 1). The mutation Q61L ensures that Rac1 is permanently in a GTP-bound, constitutively active state. Thus, Trimera can bind the plasma membrane via the Rac1 polybasic domain and the prenylation of its C terminus. Therefore, Rac1Q61L could be the principal driving force in the Trimera translocation to the plasma membrane. The Trimera localization did not change when Rac1Q61L was replaced by wild-type Rac1 or the dominant negative mutant Rac1 T17N. In fact, Rac1 T17N prevents the interaction of Rac1 with their effectors but this is not related to the binding to RhoGDI as Rac1 T17N does not bind to RhoGDI[54, 55]. So, we hypothesize that RhoGDI cannot correctly bind to Rac1 in the Trimera. In addition, the PX domain of p47^{phox} also present in the Trimera can interact with phosphatidylinositol (3,4)-bisphosphate (PI(3,4)P_2) in the membrane [41] but without cell activation, the PX domain cannot bind to the membrane [56].

In COSNOX cells, Trimera elicits a continuous activity of the NADPH oxidase. It means that Trimera adopts a position allowing the activation domain of p67^{phox} to interact with gp91^{phox} and resulting in ROS production. In the following, we discuss the adequacy of the Trimera structure to trigger the observed continuous oxidase activity. During the NADPH oxidase activation process, the TPR motifs of p67^{phox} bind to Rac1-GTP. The Rac1-GTP-p67^{phox} complex facilitates interaction of gp91^{phox} with p67^{phox} via its activation domain [42]. In Trimera, Rac1-GTP (active form due to the Q61L mutation) and 1-212 aa residues of p67^{phox} are directly fused without any linker (Figure 1), making the activation domain of p67^{phox} ready to interact with gp91^{phox}, if they co-localize in the membrane and have the right orientation. It has been shown previously that p47^{phox} can also directly interact with gp91^{phox}. Regions in p47^{phox} involved in that interaction have been identified only at one site situated within the AIR domain (aa 323–342) [43]. In Trimera, only aa residues 1-286 of $p47^{phox}$ are present (from the PX domain to the C-terminus of the second SH3 domain). So, the region that has affinity for $gp91^{phox}$ is missing. However, although $p47^{phox}$ does not directly interact with $gp91^{phox}$ in COSNOX cells, it could still interact with $p22^{phox}$ by its SH3 domains that are conserved in Trimera protein. The $p47^{phox}$-$p22^{phox}$ interaction is an essential interaction that can help to find the right orientation of Trimera to dock $gp91^{phox}$ and enable ROS production.

4.2. Constitutive ROS production: how much is too much?

While low H_2O_2 levels (1–10 nM) play an important role in redox signaling, higher levels (> 100 nM) overwhelm the anti-oxidant defenses causing oxidative stress and may cause irreversible cell damage [45]. Masoud *et al.* measured with the quantitative cytochrome *c* assay that the superoxide anion production rate elicited by Trimera is 11 $nmol.min^{-1}$ for 10^7 cells [6]. Estimating that the expression elicited by Trimera started 10 h after the transfection itself (real-time observation, data not shown), we can calculate that each cell has produced 0.9 pmol of superoxide anion within 24 h after the transfection. If we hypothesize that the superoxide anions quickly dismutate into H_2O_2 and that 0.1 to 1% of H_2O_2 diffuse back into the cell, 0.009 pmol correspond to an equivalent intracellular concentration of 0.6 to 6 mM of H_2O_2 for a cell volume of 1.5 pL (cell size 30 x 10 x 5 µm). Despite the intracellular antioxidant defense, those values are in the range of a strong oxidative stress and can cause apoptosis in cells [3]. We also observed a small population of apoptotic cells in COS-7 cells likely due to the very high overexpression of Trimera at the plasma membrane that may cover the intracellular membrane leaflet and prevent the correct interaction of other membrane bound proteins.

We also reported that the constant NOX activity leads to acidification of the intracellular environment and one might wonder if the pH variation in the cytosol could also contribute to the apoptosis. It has been described that intracellular pH of apoptotic cells is more acid (typically diminished by 0.3-0.4 pH units) than that of healthy cells [46], which is consistent with our experiments. In the two major apoptotic pathways known to date, that is, the ‘mitochondria-dependent’ pathway and the ‘death receptor’ pathway, activation of a caspases has been recognized to play a pivotal role. It was shown that activation of certain caspases is mediated by cytochrome c that is released from mitochondria, when intracellular acidification occurs [47].

Other pro-apoptotic signalling pathways, such as the p38 mitogen-activated protein kinase (MAPK) pathway, might also be affected by a cytosolic acidification [46]. Taken together, we assume that the intracellular acidification may also participate to the initiation of the apoptosis pathway in our experiments. Another event that can contribute to apoptosis is lipid peroxidation.

4.3. Localized oxidations and clustering

Using AFM-IR, we were able to observe the IR signature of chemical modifications at 1740 cm^{-1}, attributed to the C=O bond, as well as at 1260-1250 cm^{-1}, 1171-1160 cm^{-1}, 1110-1100 cm^{-1} and 1020-1010 cm^{-1}, which is correlated with the increase of C-O stretching and OH bending of hydroperoxides vibration band. The measurements showed that the intensity of IR signal is directly related to the presence of the Trimera protein and correlated to its expression level. This suggests that the appearance of these bands is due to the intense NADPH oxidase activity. Reactive oxygen species can react not only with lipids, but also with DNA, RNA and proteins. The spectra were recorded by placing the AFM tip on the membrane far from the nucleus, thus oxidation products from DNA and RNA could be excluded. Furthermore, proteins are intricate as oxidation targets, considering 20 different side chains plus the backbone. There are many oxidation pathways that can occur leading to high complexity of products that are formed [48]. On the other hand, lipids have a more limited number of oxidation products and they can massively contribute to the signal at 1740 cm^{-1} [33, 34, 35, 49]. We cannot exclude the participation to the IR signal of oxidized forms of proteins, but the strong contribution of lipids from the membrane is expected to be predominant.

Interestingly, the signal at 1740 cm^{-1} was detected in organized hotspots with diameter ~ 200 nm. This finding is coherent with our result showing the Trimera clustering in the plasma membrane observed by FRET-FLIM. Recently, using *d*STORM super-resolution microscopy Joly *et al.* not only showed that the catalytic subunits (gp91^{phox}) also clustered in the plasma membrane, but they were able to determine the size of the clusters around 60 nm [50].

Technically, notions of clustered distribution of the NADPH oxidase were documented by immunoelectron microscopy already in 1997 [51]. Nowadays, clustering phenomenon seems to be involved in cell signaling hubs and pathways. Co-clustering of the Trimera with gp91^{phox} probably leads to a localized and very intense ROS production leading to the IR signal patches. To evaluate the size of Trimera clusters and understand their role in the formation of the oxidized lipids spots in the plasma membrane, further experiments are needed. Besides, we should also notice that Holman *et al.* investigating lung fibroblasts at different points of their cell cycle and assigned the increase of the IR band at 1740 cm^{-1} to the cells undergoing apoptosis or to already dead cells [52]. This is coherent with our results showing that about 35% of COSNOX cells expressing Trimera become apoptotic.

5. CONCLUSION

Our study validated Trimera protein as a suitable tool to simulate the NOX2 active state in living cells. It enables exclusive investigation of the NADPH oxidase in its active phase and can be considered as a potential tool for screening of inhibitors, which are NOX2-isoform specific. Our data suggest that the Trimera forms clusters and that the NADPH oxidase activity is targeted to very local spots in the cell membrane. Nonetheless, we showed that its upregulation influences overall cell physiology and function.

REFERENCES

[1] H. Buvelot, V. Jaquet, and K. H. Krause, “Mammalian NADPH oxidases,” in *Methods in Molecular Biology*, 2019. doi: 10.1007/978-1-4939-9424-3_2.

[2] L. Nault, L. Bouchab, S. Dupré-Crochet, O. Nüße, and M. Erard, “Environmental Effects on Reactive Oxygen Species Detection-Learning from the Phagosome,” *Antioxidants and Redox Signaling*. 2016. doi: 10.1089/ars.2016.6747.

[3] S. Dupré-Crochet, M. Erard, and O. Nüβe, “ROS production in phagocytes: why, when, and where?,” *Journal of Leukocyte Biology*, 2013, doi: 10.1189/jlb.1012544.

[4] H. Sumimoto, R. Minakami, and K. Miyano, “Soluble Regulatory Proteins for Activation of NOX Family NADPH Oxidases,” 2019, pp. 121–137. doi: 10.1007/978-1-4939-9424-3_8.

[5] Y. Berdichevsky, A. Mizrahi, Y. Ugolev, S. Molshanski-Mor, and E. Pick, “Tripartite chimeras comprising functional domains derived from the cytosolic NADPH oxidase components p47phox, p67phox, and Rac1 elicit activator-independent superoxide production by phagocyte membranes: An essential role for anionic membrane phospholipid,” *Journal of Biological Chemistry*, 2007, doi: 10.1074/jbc.M701497200.

[6] R. Masoud *et al.*, “Conversion of NOX2 into a constitutive enzyme in vitro and in living cells, after its binding with a chimera of the regulatory subunits,” *Free Radical Biology and Medicine*, 2017, doi: 10.1016/j.freeradbiomed.2017.10.376.

[7] A. Mizrahi, Y. Berdichevsky, P. J. Casey, and E. Pick, “A prenylated p47phox-p67phox-Rac1 chimera is a quintessential NADPH oxidase activator: Membrane association and functional capacity,” *Journal of Biological Chemistry*, 2010, doi: 10.1074/jbc.M110.113779.

[8] M. O. Price, L. C. McPhail, J. D. Lambeth, C.-H. Han, U. G. Knaus, and M. C. Dinauer, “Creation of a genetic system for analysis of the phagocyte respiratory burst: high-level reconstitution of the NADPH oxidase in a nonhematopoietic system,” *Blood*, vol. 99, no. 8, pp. 2653–2661, Apr. 2002, doi: 10.1182/blood.V99.8.2653.

[9] L. Yu, L. Zhen, and M. C. Dinauer, “Biosynthesis of the phagocyte NADPH oxidase cytochrome b558. Role of heme incorporation and heterodimer formation in maturation and stability of gp91(phox) and p22(phox) subunits,” *Journal of Biological Chemistry*, 1997, doi: 10.1074/jbc.272.43.27288.

[10] A. el Chemaly, Y. Okochi, M. Sasaki, S. Arnaudeau, Y. Okamura, and N. Demaurex, “VSOP/Hv1 proton channels sustain calcium entry, neutrophil migration, and superoxide production by limiting cell depolarization and acidification,” *Journal of Experimental Medicine*, 2010, doi: 10.1084/jem.20091837.

[11] J. Demšar *et al.*, “Orange: Data mining toolbox in python,” *Journal of Machine Learning Research*, 2013.

[12] M. Erard *et al.*, “Minimum set of mutations needed to optimize cyan fluorescent proteins for live cell imaging,” *Molecular BioSystems*, 2013, doi: 10.1039/c2mb25303h.

[13] R. Grailhe *et al.*, “Monitoring protein interactions in the living cell through the fluorescence decays of the cyan fluorescent protein,” *ChemPhysChem*, 2006, doi: 10.1002/cphc.200600057.

[14] S. Poëa-Guyon, H. Pasquier, F. Mérola, N. Morel, and M. Erard, “The enhanced cyan fluorescent protein: A sensitive pH sensor for fluorescence lifetime imaging,” *Analytical and Bioanalytical Chemistry*, 2013, doi: 10.1007/s00216-013-6860-y.

[15] L. G. Zachariassen, L. Katchan, A. G. Jensen, D. S. Pickering, A. J. R. Plested, and A. S. Kristensen, “Structural rearrangement of the intracellular domains during AMPA receptor activation,” *Proceedings of the National Academy of Sciences of the United States of America*, 2016, doi: 10.1073/pnas.1601747113.

[16] C. S. Ziegler *et al.*, “Quantitative live-cell imaging and 3D modeling reveal critical functional features in the cytosolic complex of phagocyte NADPH oxidase,” *Journal of Biological Chemistry*, 2019, doi: 10.1074/jbc.RA118.006864.

[17] M. O. Price, S. J. Atkinson, U. G. Knaus, and M. C. Dinauer, “Rac activation induces NADPH oxidase activity in transgenic COSphox cells, and the level of superoxide production is exchange factor-dependent,” *Journal of Biological Chemistry*, 2002, doi: 10.1074/jbc.M200061200.

[18] M. Sathyamoorthy, I. de Mendez, A. G. Adams, and T. L. Leto, “p40(phox) down-regulates NADPH oxidase activity through interactions with its SH3 domain,” *Journal of Biological Chemistry*, 1997, doi: 10.1074/jbc.272.14.9141.

[19] L. R. Lopes *et al.*, “Phosphorylated p40PHOX As A Negative Regulator of NADPH Oxidase,” *Biochemistry*, 2004, doi: 10.1021/bi035636s.

[20] C. C. Lanning, R. Ruiz-Velasco, and C. L. Williams, “Novel mechanism of the co-regulation of nuclear transport of SmgGDS and Rac1,” *Journal of Biological Chemistry*, 2003, doi: 10.1074/jbc.M211286200.

[21] T. Ueyama *et al.*, “Isoform-Specific Membrane Targeting Mechanism of Rac during FcγR-Mediated Phagocytosis: Positive Charge-Dependent and Independent Targeting Mechanism of Rac to the Phagosome,” *The Journal of Immunology*, 2005, doi: 10.4049/jimmunol.175.4.2381.

[22] D. Morgan, V.V. Cherny, M.O. Price, M.C. Dinauer, and T.E. DeCoursey, “Absence of Proton Channels in COS-7 Cells Expressing Functional NADPH Oxidase Components,” *J Gen Physiol*, vol. 119, pp. 571–580, 2002.

[23] B. Halliwell, “Free radicals and antioxidants - Quo vadis?,” *Trends in Pharmacological Sciences*. 2011. doi: 10.1016/j.tips.2010.12.002.

[24] G. Poli, R. J. Schaur, W. G. Siems, and G. Leonarduzzi, “4-Hydroxynonenal: A membrane lipid oxidation product of medicinal interest,” *Medicinal Research Reviews*. 2008. doi: 10.1002/med.20117.

[25] R. H. Sills, D. J. Moore, and R. Mendelsohn, “Erythrocyte peroxidation: Quantitation by fourier transform infrared spectroscopy,” *Analytical Biochemistry*, 1994, doi: 10.1006/abio.1994.1149.

[26] M. M. Gaschler and B. R. Stockwell, “Lipid peroxidation in cell death,” *Biochemical and Biophysical Research Communications*. 2017. doi: 10.1016/j.bbrc.2016.10.086.

[27] S. Dalleau, M. Baradat, F. Guéraud, and L. Huc, “Cell death and diseases related to oxidative stress:4-hydroxynonenal (HNE) in the balance,” *Cell Death and Differentiation*. 2013. doi: 10.1038/cdd.2013.138.

[28] E. Niki, “Lipid peroxidation: Physiological levels and dual biological effects,” *Free Radical Biology and Medicine*, vol. 47, no. 5, pp. 469–484, Sep. 2009, doi: 10.1016/j.freeradbiomed.2009.05.032.

[29] A. Dazzi and C. B. Prater, “AFM-IR: Technology and applications in nanoscale infrared spectroscopy and chemical imaging,” *Chemical Reviews*. 2017. doi: 10.1021/acs.chemrev.6b00448.

[30] P. Lasch and D. Naumann, “Spatial resolution in infrared microspectroscopic imaging of tissues,” *Biochimica et Biophysica Acta (BBA) - Biomembranes*, vol. 1758, no. 7, pp. 814–829, Jul. 2006, doi: 10.1016/j.bbamem.2006.06.008.

[31] M. J. Baker *et al.*, “Using Fourier transform IR spectroscopy to analyze biological materials,” *Nature Protocols*, vol. 9, no. 8, pp. 1771–1791, Aug. 2014, doi: 10.1038/nprot.2014.110.

[32] A. Reis and C. M. Spickett, “Chemistry of phospholipid oxidation,” *Biochimica et Biophysica Acta - Biomembranes*. 2012. doi: 10.1016/j.bbamem.2012.02.002.

[33] B. Vileno, S. Jeney, A. Sienkiewicz, P. R. Marcoux, L. M. Miller, and L. Forró, “Evidence of lipid peroxidation and protein phosphorylation in cells upon oxidative stress photo-generated by fullerols,” *Biophysical Chemistry*, 2010, doi: 10.1016/j.bpc.2010.09.004.

[34] F. S. Ruggeri *et al.*, “Identification of oxidative stress in red blood cells with nanoscale chemical resolution by infrared nanospectroscopy,” *International Journal of Molecular Sciences*, 2018, doi: 10.3390/ijms19092582.

[35] A. Vargas-Caraveo, H. Castillo-Michel, G. E. Mejia-Carmona, D. G. Pérez-Ishiwara, M. Cotte, and A. Martínez-Martínez, “Preliminary studies of the effects of psychological stress on circulating lymphocytes analyzed by synchrotron radiation based-Fourier transform infrared microspectroscopy,” *Spectrochimica Acta - Part A: Molecular and Biomolecular Spectroscopy*, 2014, doi: 10.1016/j.saa.2014.02.148.

[36] D. A. Zacharias, J. D. Violin, A. C. Newton, and R. Y. Tsien, “Partitioning of lipid-modified monomeric GFPs into membrane microdomains of live cells,” *Science*, 2002, doi: 10.1126/science.1068539.

[37] A. K. Kenworthy, N. Petranova, and M. Edidin, “High-resolution FRET microscopy of cholera toxin B-subunit and GPI- anchored proteins in cell plasma membranes,” *Molecular Biology of the Cell*, 2000, doi: 10.1091/mbc.11.5.1645.

[38] A. K. Kenworthy, “Peering inside lipid rafts and caveolae,” *Trends Biochem Sci*, vol. 27, pp. 435–437, 2002.

[39] R. Zidovetzki and I. Levitan, “Use of cyclodextrins to manipulate plasma membrane cholesterol content: Evidence, misconceptions and control strategies,” *Biochimica et Biophysica Acta - Biomembranes*. 2007. doi: 10.1016/j.bbamem.2007.03.026.

[40] B. D. Lam and P. L. Hordijk, “The Rac1 hyper variable region in targeting and signaling-a tail of many stories,” *Small GTPases*, 2013, doi: 10.4161/sgtp.23310.

[41] H. Valenta, M. Erard, S. Dupré-Crochet, and O. Nüsse, “The NADPH oxidase and the phagosome,” in *Molecular and Cellular Biology of Phagocytosis*, M. B. Hallett, Ed. Springer Nature Switzerland AG, 2020, p. 189.

[42] G. Karimi, C. Houée Levin, M. C. Dagher, L. Baciou, and T. Bizouarn, “Assembly of phagocyte NADPH oxidase: A concerted binding process?,” *Biochimica et Biophysica Acta - General Subjects*, 2014, doi: 10.1016/j.bbagen.2014.07.022.

[43] F. R. DeLeo, W. M. Nauseef, A. J. Jesaitis, J. B. Burritt, R. A. Clark, and M. T. Quinn, “A domain of p477phox that interacts with human neutrophil flavocytochrome b558,” *Journal of Biological Chemistry*, 1995, doi: 10.1074/jbc.270.44.26246.

[44] K. N. Maxwell, Y. Zhou, and J. F. Hancock, “Rac1 Nanoscale Organization on the Plasma Membrane Is Driven by Lipid Binding Specificity Encoded in the Membrane Anchor,” *Molecular and Cellular Biology*, vol. 38, no. 18, Jul. 2018, doi: 10.1128/MCB.00186-18.

[45] H. Sies, “Hydrogen peroxide as a central redox signaling molecule in physiological oxidative stress: Oxidative eustress,” *Redox Biology*, vol. 11, pp. 613–619, Apr. 2017, doi: 10.1016/j.redox.2016.12.035.

[46] D. Lagadic-Gossmann, L. Huc, and V. Lecureur, “Alterations of intracellular pH homeostasis in apoptosis: Origins and roles,” *Cell Death and Differentiation*. 2004. doi: 10.1038/sj.cdd.4401466.

[47] S. Matsuyama, J. Llopis, Q. L. Deveraux, R. Y. Tsien, and J. C. Reed, “Changes in intramitochondrial and cytosolic pH: Early events that modulate caspase activation during apoptosis,” *Nature Cell Biology*, 2000, doi: 10.1038/35014006.

[48] M. J. Davies, “The oxidative environment and protein damage,” *Biochimica et Biophysica Acta - Proteins and Proteomics*. 2005. doi: 10.1016/j.bbapap.2004.08.007.

[49] J. L. R. Arrondo and F. M. Goñi, “Infrared studies of protein-induced perturbation of lipids in lipoproteins and membranes,” *Chemistry and Physics of Lipids*, 1998, doi: 10.1016/S0009-3084(98)00080-2.

[50] J. Joly *et al.*, “Membrane Dynamics and Organization of the Phagocyte NADPH Oxidase in PLB-985 Cells,” *Frontiers in Cell and Developmental Biology*, vol. 8, p. 1295, Nov. 2020, doi: 10.3389/fcell.2020.608600.

[51] F. B. Wientjes, A. W. Segal, and J. H. Hartwig, “Immunoelectron microscopy shows a clustered distribution of NADPH oxidase components in the human neutrophil plasma membrane,” *Journal of Leukocyte Biology*, 1997, doi: 10.1002/jlb.61.3.303.

[52] H. Y. N. Holman, M. C. Martin, E. A. Blakely, K. Bjornstad, and W. R. Mckinney, “IR spectroscopic characteristics of cell cycle and cell death probed by synchrotron radiation based Fourier transform IR spectromicroscopy,” *Biopolymers - Biospectroscopy Section*, 2000, doi: 10.1002/1097-0282(2000)57:6<329::AID-BIP20>3.0.CO;2-2.

[53] K. Sandrock, H. Bielek, K. Schradi, G. Schmidt, and N. Klugbauer, “The Nuclear Import of the Small GTPase Rac1 is Mediated by the Direct Interaction with Karyopherin α2,” *Traffic*, vol. 11, no. 2, pp. 198–209, Feb. 2010, doi: 10.1111/j.1600-0854.2009.01015.x.

[54] K.-W. Wong, S. Mohammadi, and R. R. Isberg, “Disruption of RhoGDI and RhoA Regulation by a Rac1 Specificity Switch Mutant,” *Journal of Biological Chemistry*, vol. 281, no. 52, pp. 40379–40388, Dec. 2006, doi: 10.1074/jbc.M605387200.

[55] J. Majolée, F. Podieh, P. L. Hordijk, and I. Kovačević, “The interplay of Rac1 activity, ubiquitination and GDI binding and its consequences for endothelial cell spreading,” *PLOS ONE*, vol. 16, no. 7, p. e0254386, Jul. 2021, doi: 10.1371/journal.pone.0254386.

[56] R. V. Stahelin, A. Burian, K. S. Bruzik, D. Murray, and W. Cho, “Membrane Binding Mechanisms of the PX Domains of NADPH Oxidase p40 and p47,” *Journal of Biological Chemistry*, vol. 278, no. 16, pp. 14469–14479, Apr. 2003, doi: 10.1074/jbc.M212579200.